Perspective: Differential dynamic microscopy extracts multi-scale activity in complex fluids and biological systems

Roberto Cerbino, and Pietro Cicuta

Articles you may be interested in

Perspective: Surface freezing in water: A nexus of experiments and simulations
The Journal of Chemical Physics **147**, 060901 (2017); 10.1063/1.4985879

Communication: Hypothetical ultralow-density ice polymorphs
The Journal of Chemical Physics **147**, 091101 (2017); 10.1063/1.4994757

The expanding applications and untapped potential of differential dynamic microscopy
Scilight **2017**, 130001 (2017); 10.1063/1.5004554

Pair 2-electron reduced density matrix theory using localized orbitals
The Journal of Chemical Physics **147**, 084101 (2017); 10.1063/1.4999423

Communication: Charge transfer dominates over proton transfer in the reaction of nitric acid with gas-phase hydrated electrons
The Journal of Chemical Physics **147**, 101101 (2017); 10.1063/1.4999392

Perspective: Outstanding theoretical questions in polymer-nanoparticle hybrids
The Journal of Chemical Physics **147**, 020901 (2017); 10.1063/1.4990501

Perspective: Differential dynamic microscopy extracts multi-scale activity in complex fluids and biological systems

Roberto Cerbino[1,a)] and Pietro Cicuta[2,a)]
[1]*Department of Medical Biotechnology and Translational Medicine, University of Milan, Segrate 20090, Italy*
[2]*Cavendish Laboratory, University of Cambridge, Cambridge CB3 0HE, United Kingdom*

Differential dynamic microscopy (DDM) is a technique that exploits optical microscopy to obtain local, multi-scale quantitative information about dynamic samples, in most cases without user intervention. It is proving extremely useful in understanding dynamics in liquid suspensions, soft materials, cells, and tissues. In DDM, image sequences are analyzed via a combination of image differences and spatial Fourier transforms to obtain information equivalent to that obtained by means of light scattering techniques. Compared to light scattering, DDM offers obvious advantages, principally (a) simplicity of the setup; (b) possibility of removing static contributions along the optical path; (c) power of simultaneous different microscopy contrast mechanisms; and (d) flexibility of choosing an analysis region, analogous to a scattering volume. For many questions, DDM has also advantages compared to segmentation/tracking approaches and to correlation techniques like particle image velocimetry. The very straightforward DDM approach, originally demonstrated with bright field microscopy of aqueous colloids, has lately been used to probe a variety of other complex fluids and biological systems with many different imaging methods, including dark-field, differential interference contrast, wide-field, light-sheet, and confocal microscopy. The number of adopting groups is rapidly increasing and so are the applications. Here, we briefly recall the working principles of DDM, we highlight its advantages and limitations, we outline recent experimental breakthroughs, and we provide a perspective on future challenges and directions. DDM can become a standard primary tool in every laboratory equipped with a microscope, at the very least as a first bias-free automated evaluation of the dynamics in a system. *Published by AIP Publishing.* [http://dx.doi.org/10.1063/1.5001027]

I. INTRODUCTION

For about 50 years, since the development of affordable laboratory laser sources, it has been possible to perform dynamic light scattering (DLS) experiments. This technique enabled a huge swathe of discoveries: from the universal behavior of mixtures close to criticality, to the general properties of motion of macromolecules such as polymers and colloidal particles.[1–3] DLS uses optics (selecting one scattering angle and collecting light in the far field) to probe a particular scattering wave-vector in the system: the temporal autocorrelation of the intensity of the scattered light characterizes the time scale(s) over which the sample restructures itself on the length scale (wave-length) that corresponds to the chosen wave-vector. By acquiring data on a range of scattering angles (typically in a series of measurements, at the expense of longer experimental durations), one can recover in principle a very complete picture of relaxation processes across the different length scales.

Only more recently, in the last 20 years or so, computers and digitization of images made it feasible to capture time-lapse sequences and, from these, to extract quantitative parameters of the dynamics. In the context that we focus on here, i.e., soft matter and biological systems, these movies are typically recorded through an optical microscope setup. Two broad approaches have been either (i) segmenting the images to extract features, and then building trajectories of these features over time, or (ii) performing correlations across the timecourse, to extract velocity maps. The first approach is typical both in biology experiments[4–6] and in "microrheology"[7] (tracer particles can be used as local probes of the mechanics in a material). The second approach is typical in fluid dynamics[8] and in experiments probing displacement fields.[9,10] The progress both in computational power and even more strikingly in digital image sensors has led microscopy approaches to become the conventional experimental tool. Furthermore, many samples of interest are available only in very small volumes, or as thin quasi two-dimensional materials (e.g., cell cultures), and these are not compatible with traditional dynamic light scattering approaches. However, this move to "real space" analysis poses serious challenges: segmentation is very often difficult and computationally expensive, it requires case-by-case fine tuning, it is sometimes just impossible to automate, as in dense systems; the correlation-based approaches wash out many types of motion (e.g., random fluctuations and displacements) and can therefore intrinsically be deployed only in very selected situations.

In 2008, a revolutionary method was proposed by Cerbino and Trappe:[11] Differential Dynamic Microscopy (DDM). The power of this method as a modern alternative to DLS was immediately explained, but the impact and the range of

---
a)Authors to whom correspondence should be addressed: roberto.cerbino@unimi.it and pc245@cam.ac.uk

discovery made possible by this approach became clear in the last decade and are still being explored by an increasing number of adopters. Implementing DDM does not require advanced high-end optics; consumer-led demand for its two underlying technologies (computing and digital cameras) is rapidly propelling it forwards in terms of speed and power; with small variations, DDM has been shown to extract a whole set of parameters typical of the traditional approaches outlined above, and more.

This perspective aims to capture the research made possible by DDM in its first decade, including mostly very recent developments, and to suggest untapped potential areas where it could be fruitful. We particularly highlight the questions and challenges posed by systems with "multiscale dynamics," of which there are many important examples both in complex fluids (e.g., gel networks) and biology (e.g., cell tissues). To make a very concrete example from living systems, one wants to isolate intracellular motions from the motions of cells themselves, and even if focusing on cell motion, it is often the case that the character of motion changes across a time or length scale, as persistence is lost (e.g., in run and tumble bacterial motility dynamics). These are typical scenarios where the DDM approach is ideal.

II. BASIC PRINCIPLES OF DDM

We do not replicate here the detailed treatment of image formation through the optical system; this is necessary for a full understanding of the DDM signal output. Readers interested in details and early applications of the technique can refer to Refs. 12 and 13, where DDM was discussed in the framework of near field scattering and digital Fourier microscopy, respectively. We take here a slightly more empirical approach, which most adopters are likely to find sufficient for a "first pass" to quantify dynamics in their system; readers can trust this is rigorous by referring to several cases where there has been in-depth analysis. The key of the DDM analysis is the differential signal $d(\vec{r}, t_0, \tau)$ obtained by subtracting two images acquired at different time, the first one at time t_0 and the second one at time $t_0 + \tau$,

$$d(\vec{r}, t_0, \tau) = I(\vec{r}, t_0 + \tau) - I(\vec{r}, t_0), \qquad (1)$$

where besides its time dependence, I encodes the image intensity as a function of the position $\vec{r} = (x, y)$ in the microscope image and the optical axis is along z. By calculating the spatial 2D Fourier transform $d(\vec{q}, t_0, \tau)$ of the differential signal and squaring it, we obtain the so-called image structure function

$$D(\vec{q}, \tau) = \left\langle |d(\vec{q}, t_0, \tau)|^2 \right\rangle_{t_0}, \qquad (2)$$

where $\vec{q} = (q_x, q_y)$ is the wave-vector in the Fourier space and where the average over t_0 is made for stationary or quasistationary dynamics to increase the statistical accuracy of the image structure function (we discuss in Sec. III G an interesting application of DDM, in which such average is not performed). A wave-vector q corresponds in real-space to a sinusoidal modulation with wavelength $\Lambda = 2\pi/q$. In this article, we will refer to Λ as the "length scale" probed by a particular q-mode.

It can be shown[11,13–17] that the image structure function takes the general form

$$D(\vec{q}, \tau) = A(\vec{q})[1 - f(\vec{q}, \tau)] + B(\vec{q}), \qquad (3)$$

where the function $f(\vec{q}, \tau)$ is known as the normalized "Intermediate Scattering Function," as commonly measured in DLS experiments.[1] This function $f(\vec{q}, \tau)$ encodes the cumulative probability that the displacement of a material element over time τ will lie within a distance equal to the length scale Λ encoded by q. Thus $f(\vec{q}, \tau)$ characterises how quickly structure is "lost" over a length scale $\sim 1/q$; it will decay to zero for samples that lose memory of their structure, over sufficiently long times, for instance because of diffusion or flow. In general, the greater the q, the faster the decay of $f(\vec{q}, \tau)$ and the less the time to reach the saturation level in $D(\vec{q}, \tau)$. $A(\vec{q})$ and $B(\vec{q})$ are the functions related to the static scattering properties of the sample, to the details of the imaging process optics and to the noise in the acquisition. In many cases, they are assumed to be merely fitting parameters even though with proper treatment important information can be extracted from their study. For instance, in Refs. 18–20, quantitative static scattering information was successfully extracted from the DDM analysis.

The dynamics of many systems are completely captured by $f(\vec{q}, \tau)$ and the basic principle, and power, of DDM is how an image stack can be processed and related to $f(\vec{q}, \tau)$ as in Eq. (3). For completeness, we should mention that systems where $f(\vec{q}, \tau)$ fails to be a useful characterization do exist, for example, non-stationary evolving systems must be handled differently and we touch on some of these later. In a vast number of cases, where the system has dynamics around thermodynamic equilibrium or where there is a well-defined stationary state, then $f(\vec{q}, \tau)$ is very meaningful. In practice, how to proceed from Eq. (3) depends on how much is already known about the character of dynamics in the given experiment, and on the source of contrast in the images. In the following, unless specified we will consider systems for which the image structure function $D(\vec{q}, \tau)$ is azimuthally isotropic in the $\vec{q}$ plane. We can thus make use of the azimuthal average $D(q, \tau)$ of the image structure function and note that Eq. (3) remains valid provided that we replace everywhere $\vec{q}$ with its magnitude $q = \sqrt{q_x^2 + q_y^2}$. From this process, we typically have D calculated for $N/2$ Fourier modes, from an image of $N \times N$ pixels.

The simplest scenario, and the one where DDM is being widely adopted, also in teaching laboratories,[21] is in experiments where either tracer particles are added into a material for characterizing its dynamics or through fluorescent tagging, it is possible to achieve an image in which the signal is related to a known structural element (e.g., an organelle in a cell or the whole cell in the context of cell motility). This is then analogous to microrheology by particle tracking,[7,22] but DDM has several advantages (and many of the same limitations). In this scenario, the intermediate scattering function is determined by the motion of the tracers (or fluorescent species) and the image "restructures" over a given length scale in a time related to how long it takes these tracers to move that typical distance. The average motion of tracers can be represented by their mean square displacement

$\langle r^2(\tau)\rangle = \langle x^2(\tau) + y^2(\tau) + z^2(\tau)\rangle = \langle x_\perp^2(\tau) + z^2(\tau)\rangle$, and for small wave-vectors and in conditions for which the distribution of displacements is Gaussian, we have

$$D(q,\tau) = A(q)\left[1 - e^{-\frac{q^2}{4}\langle x_\perp^2(\tau)\rangle}\right] + B(q). \qquad (4)$$

The mean square displacement follows well known physics in the case of diffusion, $\langle x_\perp^2(\tau)\rangle = 4D_T\tau$ (where D_T is the translational diffusion coefficient), which leads to

$$D(q,\tau) = A(q)\left[1 - e^{-D_T q^2 \tau}\right] + B(q). \qquad (5)$$

In the simplest Newtonian fluid case (Fig. 1), $f(q,\tau)$ is just the exponential function in Eq. (5). In general, the time dependence of $D(q,\tau)$ for objects in non-Newtonian (i.e., viscoelastic) or hindered motion backgrounds is more complex but can be fitted with an appropriate function of τ (the same for all q although with possibly q-dependent coefficients) from which the fluid parameters can be measured. If the sample is Newtonian, one measures the diffusion coefficient (and thus particle size or fluid viscosity, if the other is known); if the dynamics is sub-diffusive or super-diffusive with a power law dependency, one recovers the power law exponent.[23]

In more complex scenarios, one perhaps has much less knowledge of the dynamics in the system and/or less control over the source of the optical contrast in the images. DDM is extremely powerful in this scenario too: an empirical

approach to the data is possible, for example, fitting $f(q,\tau)$ as an exponential, the underlying assumption being that one searches for a typical time scale associated with restructuring over a certain length scale, but without the prior knowledge of the underlying process. This approach can provide the general character of the dynamics in the system. As an example, imagine a suspension of particles, which might be passive (undergoing Brownian motion) or active (moving with ballistic motion). In Brownian motion $\langle x_\perp^2(\tau)\rangle \sim D_T\tau$, whereas for ballistic motion, such as bacteria swimming in a run phase with velocity v, we have $\langle x_\perp^2(\tau)\rangle \sim (v\tau)^2$. For each q, the fitting of $D(q,\tau)$ will provide a different characteristic time scale $\tau_c(q)$. Dimensional analysis of these two relations of mean square displacement [given that $\langle x_\perp^2(\tau)\rangle \sim 1/q^2$] leads to an expectation that $\tau_c(q) \sim 1/q^2$ for Brownian motion, and $\tau_c(q) \sim 1/q$ for ballistic motion. This is indeed observed in DDM signals, analyzed in this empirical fashion, showing that the type of motion in the system can be extracted in the absence of a detailed model. Note that in this particular example of bacterial motility, a detailed model for $f(q,\tau)$ was known from DLS[1] and has been applied in DDM experiments;[24] with such a detailed model, one has the correct form of $f(q,\tau)$, in this case as a function of the velocity v, which can therefore be measured exactly.

In common with particle tracking and DLS approaches, one must obviously be aware of confinement effects, for
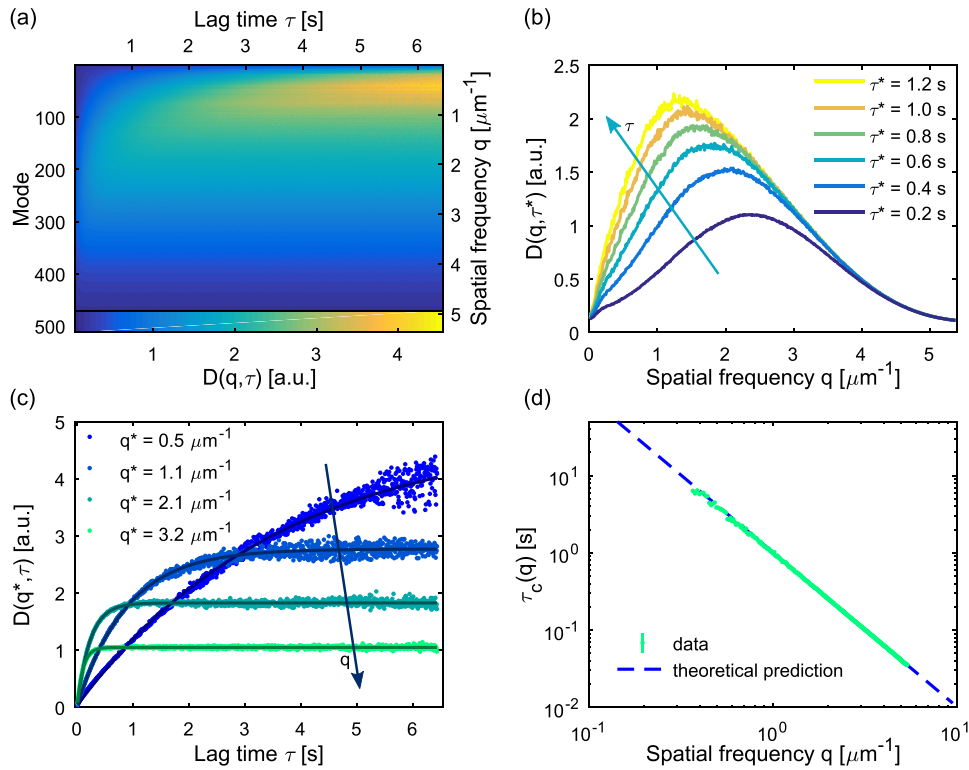

FIG. 1. DDM analysis of colloidal particles shows they undergo Brownian motion and measures the diffusion coefficient. Movies of 4670 frames are taken with a Grasshopper CMOS camera, at 181 fps, with a 10× objective NA = 0.3, where 1 camera pixel corresponds to 0.584 μm. The particles are carboxylated polystyrene particles, radius a = 250 nm, Bangs Laboratories Inc., Bangs Lot# 4127, Lot# L071015F, solid 0.1% (1 in 100 from 10% bottle), in water. (a) The intermediate scattering function D(q,τ) is shown for all modes and for lag times up to a quarter of the total movie time. This information is "cut" by lag time (b) and by scattering vector (c). In (c), the D(q,τ) data are fitted (solid lines) with exponential curves as in Eq. (5), yielding a relaxation time $\tau_c(q) = 1/Dq^2$. The time scales are shown in (d) in log-log scales, highlighting the inverse square dependence on the wave-vector, characteristic of Brownian motion. The dashed line in (d) is the theoretical prediction $\tau_c(q) = 1/D_T q^2$, with Stokes-Einstein diffusion coefficient $D_T = k_B T/(6\pi\eta a)$, T = 25 °C, η = 0.89 Pa s (giving $D_T = 0.98$ μm²/s; fitting that same dataset gives $D_{T,exp} = 0.988 \pm 0.002$ μm²/s).

example, the increased drag from walls. The finite focal depth also sets a maximum time scale over which sample dynamics can be observed (similarly to the fact that particle tracks would have a typical maximum length, also from finite depth of focus). This has been explored systematically in confocal microscopy[18] and in light-sheet[25] DDM experiments.

Similar to DLS, DDM is based on a model for the intermediate scattering functions. When such model is obvious, as for monodisperse or slightly polydisperse colloidal suspensions, quantitative extraction of model parameters is immediate and does not require any user input. On the contrary, when more than one model is to be evaluated for appropriateness and/or validity, the analysis might require some additional user intervention. In particular, we stress that whilst fitting and validation represent crucial steps in the DDM analysis, for these aspects, one can benefit directly from decades of previous experience of DLS users.

III. RECENT ADVANCES

In this section, we will discuss a few selected applications of DDM in which it was either used to perform otherwise difficult—if not impossible—experiments or combined with other ideas to prove new experimental approaches with a notable future potential. In selecting the material for presentation, we have restricted ourselves to very recent literature (last three years), where the standard DDM approach outlined above is sometimes extended in various ways. Various earlier studies using DDM, which follow the standard approach summarized above, are overviewed in Refs. 12 and 13.

A. Viscosity of deeply supercooled water and its coupling to molecular diffusion

A typical application of DDM is to determine the diffusion constant of colloidal particles dispersed in a liquid medium.[11,16,17,26,27] If the viscosity of the host liquid is known, DDM behaves as a powerful particle sizing tool, in that it enables one to determine accurately the size of the colloidal particles. On the other hand, if the particle size is known, DDM can be used to perform precise viscometry experiments. The latter has been shown elegantly in an application by Caupin and co-workers, who used DDM to probe the viscosity of super-cooled liquid water close to the limit of homogeneous crystallization.[28] Since water is a poor glass-former, measuring its viscosity in the super-cooled state is a challenging feat that requires avoiding crystallization. DDM was used to probe the diffusivity of tracer polystyrene spheres with radius $a = 175 \pm 3$ nm. Curves of the correlation time τ as a function of the wave-vector q were found to be well fitted by $\tau(q) = (D_T q^2)^{-1}$ for all temperatures. The authors were thus able to estimate the super-cooled water viscosity in the deeply quenched regime (down to −34 °C).

The data obtained by Caupin and co-workers show clearly that the only model that describes the water viscosity for all the available temperature values is the power-law viscosity model (it appears to be superior to other possible models such as the Arrhenius, the parabolic, or the Vogel–Fulcher–Tammann models), see Fig. 2. In addition, measuring the water viscosity in such wide temperature range proved to be crucial to test validity of the Stokes–Einstein and Stokes–Einstein–Debye relations. In analogy with molecular glass-formers, the Stokes-Einstein relation, linking viscosity to translational diffusion, is violated whereas the link between viscosity and rotational motion, expressed by the Stokes-Einstein-Debye relation, seems to remain robust. This new insight into the behavior of supercooled water was made possible by DDM, which provided unprecedented access to viscosity at very low temperatures, where previous attempts failed. In fact, the main advantages of DDM over particle tracking in these experiments are the following: (a) by using small tracer particles, DDM can make the overall length of an experiment shorter than the time over which water solidifies; and (b) by using several particles (many more than could possibly be tracked, we estimate from information in that article that a few thousand particles are in the field of view), it provides a statistically significant, user-independent determination of the dynamics. We will further comment in Sec. V about possible future developments in this area.
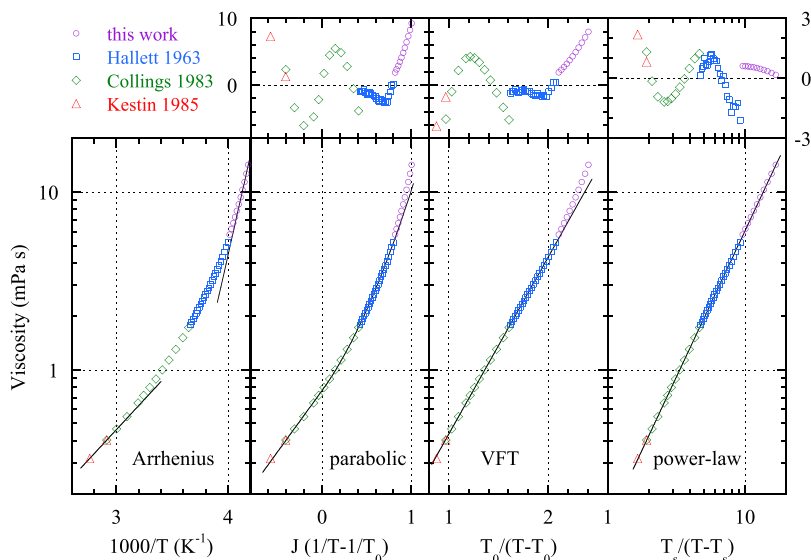

FIG. 2. Viscosity of supercooled water. Purple circles from Ref. 28, blue squares from Ref. 29, green diamonds from Ref. 30, and red triangles are from Ref. 31. (Left) Arrhenius plot, showing an apparent activation energy increasing from 1560 to 6410 K upon cooling (solid lines). (Left center) Parabolic law, with best fit (χ^2 = 14.2) parameters T_0 = 305.15 K, η_0 = 2.323×10^{-6} Pa s, J = 1112 K, and E_a = 1769 K. (Center right) Vogel–Fulcher–Tammann (VFT) representation, with best fit (χ^2 = 10.5) parameters T_0 = 168.9 K, η_0 = 4.442×10^{-5} Pa s, and B = 2.288. (Right) Power law representation, with best fit (χ^2 = 0.91) parameters T_s = 225.66 ± 0.18 K, η_0 = $(1.3788 \pm 0.0026)10^{-4}$ Pa s, and γ = 1.6438 ± 0.0052. (Top) The normalized residuals $(\eta_{exp} - \eta_{fit})/\sigma_{exp}$, where η_{exp} and η_{fit} are the experimental and fitted viscosities, respectively, and σ_{exp} is the experimental uncertainty (1 standard deviation). Note that the vertical scale of top right is different. Reproduced with permission from Dehaoui *et al.*, Proc. Natl. Acad. Sci. U. S. A. **112**, 12020 (2015). Copyright 2015 National Academy of Sciences.

B. Diffusive dynamics of nanoparticles in ultra-confined media

Two features of DDM for which DLS is easily outperformed in applications are the insensitivity to static features within the sample and the immediate access to a large number of two-dimensional wave-vectors $\vec{q} = (q_x, q_y)$. In Ref. 32, both of these features were exploited to investigate the dynamics of nanoparticles diffusing in dense arrays of nanoposts arranged on a square lattice. Owing to the use of image subtractions, DDM analysis made the nanoposts invisible and brought to light the dynamics of the confined nanoparticles, which was inspected for possible anisotropy. Remarkably, even for the most severe confinement conditions, isotropic dynamics was always observed, with intermediate scattering functions well-described by stretched exponential relaxation. The diffusion coefficient extracted from DDM was found to decrease with increasing confinement (Fig. 3).

Such a decrease was tested against available models for hindered diffusion, which incorporate steric hindrance and hydrodynamic interactions. The experimental data were found to be in agreement with two models, specifically the so-called centerline approximation and cross-sectional averaging (further details about the models can be found in Ref. 32), which make predictions for the dependence of the diffusivity on the ratio $\lambda = d_{NP}/P$ between the diameter d_{NP} of the nanoparticles and the diagonal spacing P between posts. Such agreement suggests that both steric restrictions and hydrodynamic drag may be the cause of the decreased diffusivity of nanoparticles in post arrays.

C. Anomalous dynamics of intruders in a crowded environment of mobile obstacles

Studying the dynamics of small particles of diameter σ_s coexisting with larger particles of diameter σ_l is not an easy task. Video particle tracking[33] is difficult in a crowded environment, especially if we are interested in tracking the small particles. Dynamic light scattering (DLS)[1] does not allow us to distinguish the two species in an easy way. A possibility would be to tag the particles with different fluorophores and using Fluorescence Correlation Spectroscopy (FCS)[34] to selectively probe the dynamics of each species separately. However, FCS probes the dynamics only on a length scale of the order of the measurement volume (typically ranging from some μm to a few tens of μm), which is set by the convolution of the illumination and the detection regions. FCS cannot thus probe in a simple way the rich, multi-scale dynamics expected in mixtures of colloids of different sizes. For these reasons, Sentjabrskaja *et al.*[35] used confocal DDM (ConDDM)[18] on binary mixtures of particles that were tagged with different fluorophores. The selectivity of the fluorescent labelling together with the depth selection capabilities of the confocal detection scheme enabled probing the multi-scale dynamics of these dense colloidal suspensions by focusing on the contributions of each species as a function of the volume fraction and of the size ratio $\delta = \sigma_s/\sigma_l$.

Their results, complemented with numerical simulations, show that a critical size asymmetry exists at which the onset of anomalous collective transport of the small particles is observed, as mirrored by a logarithmic decay of the intermediate scattering function at the length scales of the order of the size of the large particles (Fig. 4). Interestingly, the matrix mobility is crucial for the observed anomalous behavior. The larger and slower particles, when present at sufficiently large concentration, act as a slowly rearranging, glassy matrix. The continuous evolution of the channels in the mobile matrix alters in a profound way the dynamics of the small particles due to the thermal motion of large particles, a situation that can be found for a wide range of phenomena ranging from glassy systems to cell biology.[35]

D. Active diffusion and advection in the *Drosophila* ooplasm result from the interplay of the actin and microtubule cytoskeletons

The previous example made clear how using different fluorophores for selected objects enables a selective probing of the dynamics in crowded environments. More in general, the use of different contrast mechanisms can be beneficial in probing the multi-scale dynamics in a complex environment, such as the cell interior.[36] A significant step in this direction was taken by Drechsler *et al.*,[37] who combined ConDDM and Differential Interference Contrast DDM (DIC-DDM) to probe selectively inside a *Drosophila* oocyte, the dynamics of cytoskeletal filamentous actin (F-actin) and endogenous vesicles, respectively. During oogenesis, the oocyte is characterized by a combination of different transport mechanisms,
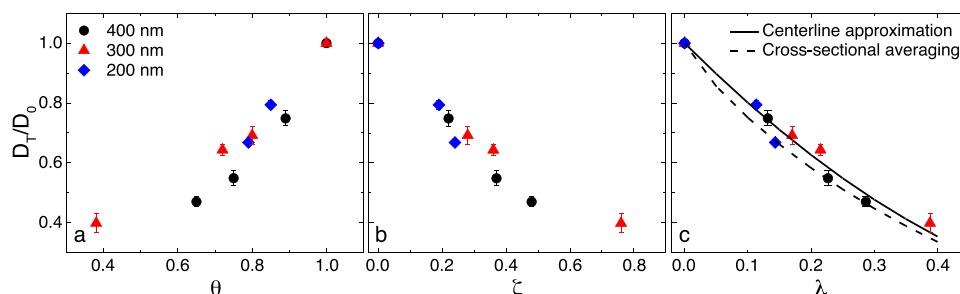

FIG. 3. Confinement affects colloidal dynamics. Relative diffusivity D_T/D_0 as a function of (a) void fraction θ and confinement parameters (b) $\zeta = d_{NP}/S$ and (c) $\lambda = d_{NP}/P$ for aqueous dispersions of nanoparticles of varying diameter, where S is the minimum spacing between posts and P is the diagonal spacing between posts. Data obtained with DDM are plotted for particles with diameter $d_{NP} = 400$ nm (black circles), 300 nm (red triangles), and 200 nm (blue diamonds). The solid and dashed black lines in (c) indicate the centerline approximation and the cross-sectional averaging expressions for diffusion in slit pores [see Eqs. (3) and (4) in Ref. 32]. Adapted with permission from Jacob *et al.*, Soft Matter **11**, 7515 (2015). Copyright 2015 The Royal Society of Chemistry.
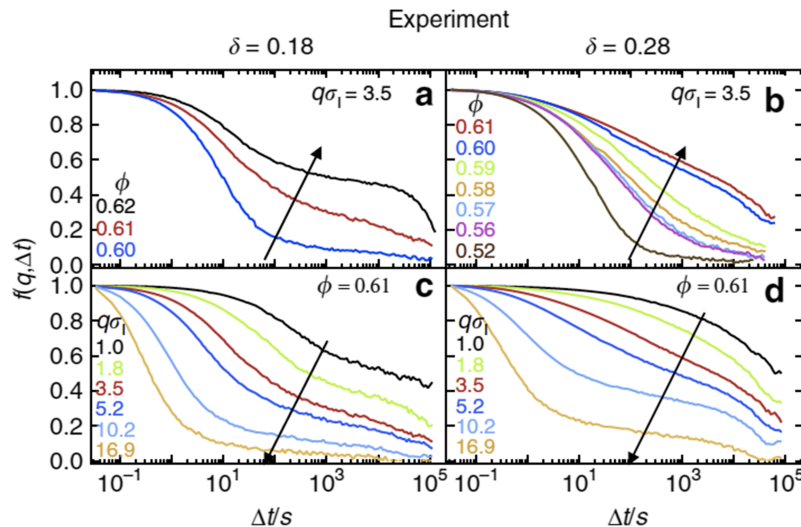
FIG. 4. Dynamics of small spheres (intruders) moving in a matrix of larger spheres. Intermediate scattering functions f(q,Δt) extracted by ConDDM for the small spheres as a function of the delay time Δt. The size ratio δ is below [(a) and (c)] and around [(b) and (d)] the onset of anomalous dynamics. Data are shown for different magnitudes of the scattering wave vector q and total volume fraction ϕ (as indicated). Arrows indicate increasing ϕ and increasing q accordingly. For δ = 0.18 and all ϕ and q, an initial decay is observed that can be associated with the Brownian motion of small particles within the voids of the large particles matrix. This decay becomes increasingly slower for increasing ϕ [Fig. 4(a)] and decreasing q, which corresponds to an increasing length scale [Fig. 4(c)]. A ϕ-dependent intermediate plateau and a final decay to zero at longer times can be also appreciated [Fig. 4(a)]. The intermediate plateau, which mirrors the temporary trapping of particles at the length scale 1/q, has a height that increases progressively with increasing ϕ, suggesting a percolation-like scenario with voids becoming smaller and particle localization stronger. The observed final decay to zero is a consequence of the long-time diffusive escape of the particles. The picture changes dramatically for larger size ratios [(b) and (d)]. When the total volume fraction ϕ is larger than 0.60, a logarithmic decay of f(q,Δt) over three decades in time is observed, in particular for $q\sigma_l = 3.5$, which corresponds to a probed length scale of about $2\sigma_l$ [Fig. 4(b)]. Reproduced with permission from Sentjabrskaja *et al.*, Nat. Commun. **7**, 11133 (2016). Copyright 2016 Author(s), licensed under a Creative Commons Attribution 4.0 License.

including directed transport by cytoplasmic flows[38] and active diffusion.[39]

While Particle Image Velocimetry (PIV) can be used to assess the directed transport of both vesicles and actin by the flow, quantifying diffusion is more difficult, especially for small (below the diffraction limits) actin filaments in a crowded environment. By contrast, DDM experiments were able to show that two cytoskeletal structures, microtubules and actin, are responsible for the cytoplasmic flow and for active diffusion, respectively. In particular, the ConDDM analysis of the cytoskeletal F-actin revealed that the motility of cytoplasmic actin filaments directly correlates with vesicle motion both in the presence and in the absence of the cytoplasmic flow (Fig. 5). While this result is somehow obvious for the directed transport, in that both vesicles and actin are transported by the cytoplasmic streaming [Fig. 5, panel (f)], way less obvious is the fact that the diffusion coefficient of actin is always twice the diffusion coefficient of the vesicles [Fig. 5, panel (g)]. This last result is compatible with the hypothesis that cytoplasmic f-actin is the source of active diffusion of the vesicles in the *Drosophila* oocyte. However, it is also found that active diffusion is reduced in oocytes lacking microtubules, which suggests that behind their well-recognized role in intracellular transport and cytoplasmic streaming, microtubules substantially contribute to active diffusion.

E. Multi-scale DDM to characterize synchronization of motile cilia

Another example of biomedical application of DDM is the recent study of collective dynamics in motile cilia. These cilia have a periodic (frequencies between a few Hz and 50 Hz)

and well-defined beating pattern, and a key open question in many systems is how multiple cilia coordinate their beating for an efficient macroscopic fluid transport, particularly across many cells. Feriani *et al.*[40] have investigated airway tissues, where in healthy physiological conditions, the neighboring cilia act as phase-locked oscillators, forming a so-called "metachronal wave" that allows a continuous clearance of mucus from the lungs. The dynamics of cilia, the metachronal wave, and the resulting directed flow that allows mucus clearance can all be observed and measured in animal sections. However, those experiments do not allow for the type of control (cell-cell position, distance, and orientation) that would enable tuning of interactions and thus to highlight the dominant mechanisms underpinning synchronization. These complications were tackled by Feriani *et al.*[40] with the use of "air-liquid interface" cultures where the cells grow on a solid permeable membrane support and are exposed to air on their apical side. A typical image taken across such a culture is shown in Fig. 6(a). Due to the supporting membrane, the cell bodies and the heterogeneities in the mucus layer, it is obvious that segmenting cilia in images like this would be incredibly challenging. For the questions of temporal and spatial coherence scales of cilia dynamics, the segmentation of cilia is not required. DDM is hence an ideal technique here: it intrinsically removes the static signal in the image, and it returns space-resolved dynamics.

A DDM analysis of the full-field returns $D(q, \tau)$ signals that have a clear frequency and a damping, Fig. 6(b). In airway cells, this cilia beating frequency (CBF) is approximately 15 Hz and is a property that could be easily probed by many different analysis approaches. The damping in the $D(q, \tau)$ data
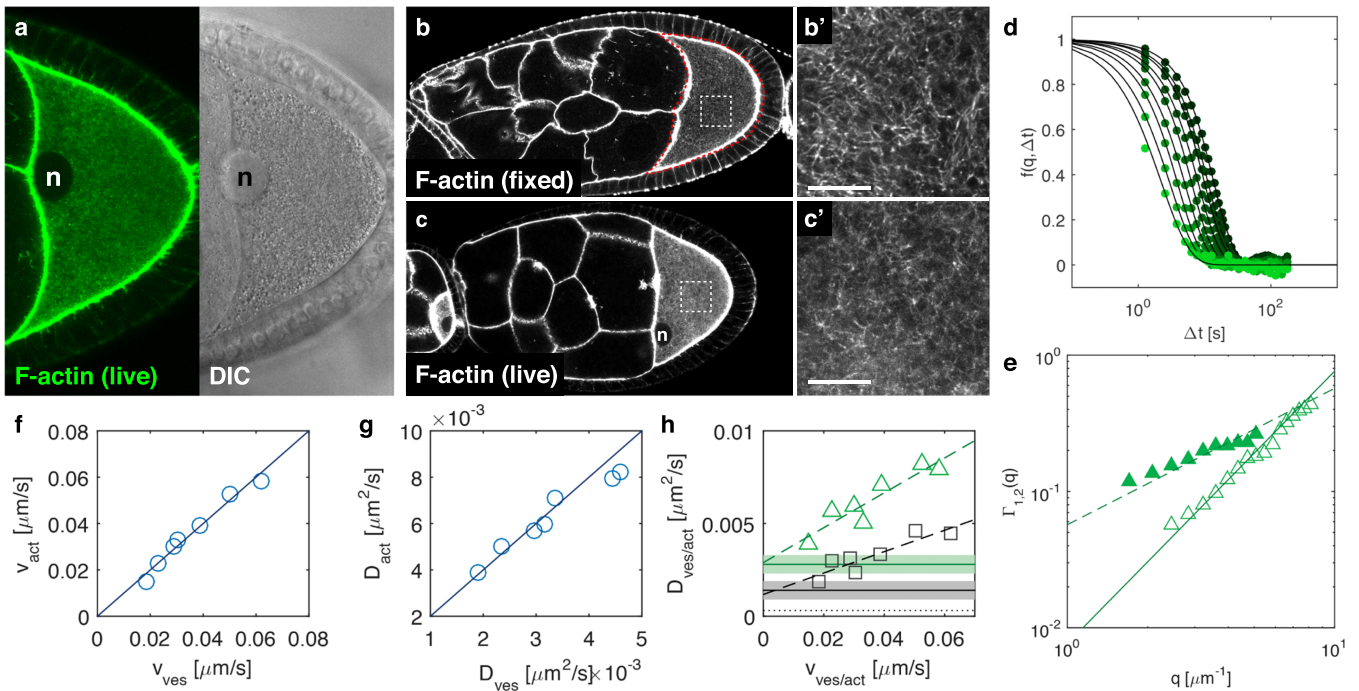
FIG. 5. In the *Drosophila* oocyte, the motion of cytoplasmic F-actin directly correlates with the motion of endogenous vesicles. (a) Image of a cell, expressing the F-actin fluorescent binding protein UTRN.GFP (left panel). DIC image of the same oocyte (right panel) n = nucleus. (b) Distribution of F-actin (stained with TRITC-phalloidin) in a fixed egg chamber. (b′) High magnification of cytoplasmic actin filaments [white box in (b)]. (c) UTRN.GFP expressing living egg chamber. UTRN.GFP labels the same structures as phalloidin in fixed samples [compare with (b)]. (c′) High magnification of cytoplasmic actin filaments in a UTRN.GFP expressing living oocyte [white box in (c)]. (d) Intermediate scattering functions f(q,Δt) obtained from the Con-DMM analysis for different wave vectors q in the range $2\,\mu m^{-1} < q < 8\,\mu m^{-1}$. Continuous lines are best fit to the prediction of a simple advection-diffusion model. (e) Decorrelation rates $\Gamma_1(q)$ (solid triangles) and $\Gamma_2(q)$ (open triangles) obtained from the fit of f(q,Δt) in (d) with a function describing a double decay with rates $\Gamma_1(q)$ and $\Gamma_2(q)$. Dashed line constitutes the best fit of $\Gamma_1(q)$ to a linear function $\Gamma_1(q) = v_{act}q$, whereas the continuous line is obtained from the fit of $\Gamma_2(q)$ to a quadratic function $\Gamma_2(q) = D_{act}q^2$. (f) Mean speeds of F-actin (v_{act}), plotted against vesicle mean speeds (v_{ves}) for different cells. The continuous line represents $v_{act} = v_{ves}$. (g) Diffusion coefficients of F-actin (D_{act}) plotted against diffusion coefficients of vesicles (D_{ves}) for different cells. The continuous line corresponds to $D_{act} = 2\,D_{ves}$. (h) D_{act} (green triangles) and D_{ves} (black boxes) as a function of the respective mean speeds v_{act} and v_{ves}. Horizontal solid lines represent $D_{act,nf}$ and $D_{ves,nf}$, obtained from colchicine treated cells, showing no persistent motion (green <-> F-actin and black <-> vesicles). Dashed areas correspond to mean value ±sd. These values agree remarkably well with the extrapolated behavior for v → 0 of the experimental data obtained from control cells (dashed lines). The horizontal dotted line corresponds to the estimated value of the thermal diffusion coefficient D_{TH} of the vesicles, characterizing their spontaneous fluctuation in the absence of any active process. Scale bars represent 10 μm. Reproduced with permission from Drechsler *et al.*, preprint bioRxiv 098590 (2017). Copyright 2017 Author(s), licensed under a Creative Commons Attribution 4.0 License.

can be caused by two effects: the loss of temporal coherence in each cilium (i.e., each cilium is not a perfect oscillator, and we can imagine a stochastic drift in its phase) or the averaging over regions that are poorly phase locked and have slightly different CBFs. We can think of these, respectively, as the synchronization scales in time and space. An extension of the standard DDM approach, which was named "multiscale DDM" was proposed to pick up separately the temporal and spatial scales of synchronization. Multiscale DDM consists of performing DDM over a whole series of different windows (tilings of the image). The authors typically choose tiles of log-spaced size, ranging from the close to full frame down to a small tile, the choice of which limits the minimum wave-vector that can be compared across tiles [in Fig. 6(c), from 480 × 480 down to 8 × 8 pixels]. Then, separate $D(q, \tau)_{tile}$ signals are obtained and can be compared. In the particular case of cilia, see Fig. 5(c), the spatial scale of phase locking reflects itself in a strong dependence of the decay times as a function of the tile size. What the analysis is picking up is the fact that locally (within 20 μm, i.e., inside the smallest tiles) cilia are strongly coupled and thus completely phase-locked, whereas at larger distances, this locking is progressively lost,

so large tiles are averaging over multiple poorly phase-locked dynamics. The resulting decay time has a sigmoidal transition as a function of tile size, highlighting a spatial scale, which in the conditions of Fig. 6(c) corresponds to a few cell diameters. This is consistent with what is known from coupling mediated by fluid flow.[41] Generally, in a system that has a spatial scale for collective or coherent motion, one expects that scale to emerge as a feature when comparing the dynamics across tile sizes. We note that again, like the basic DDM approach, multiscale DDM remains a user-free automated analysis (once a general choice is made for a family of dynamics to be searched/fitted for). We expect multiscale DDM to be useful in other dynamically heterogeneous systems, well beyond motile cilia.

F. Simultaneous characterization of rotational and translational diffusion of optically anisotropic particles

Like DLS, which studies the fluctuations in the scattered light intensity, DDM analyses the fluctuating intensity of microscopy images. Generally, these fluctuations arise from refractive index fluctuations within the sample. In typical
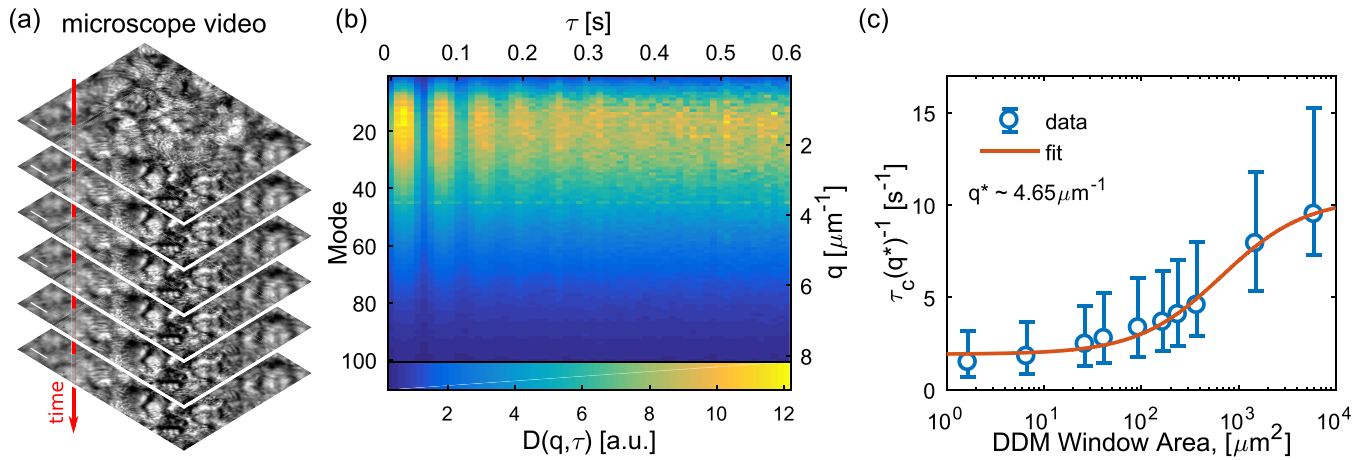
FIG. 6. Multiscale DDM can highlight the scale of dynamical spatial coherence. This approach was developed to study phase locking in carpets of motile cilia but has broader applicability. Images in these experiments (a) would be very difficult to segment. Instead, the DDM algorithm efficiently extracts D(q,τ) (b), shown here as a heatmap for the first hundred or so modes in the image, from each of which the frequency and damping of the motile cilia can be fitted. In multiscale-DDM, the DDM analysis is performed systematically on square boxes of different sizes, from the whole image down to a few pixels (the small window limits the range of wave-vectors that can be followed across the multiscale). (c) shows the decay time in the oscillations typically seen in (b) for full-field DDM, but now fixing a wave-vector and plotting as a function of the DDM window size. The inflection point of these data (corresponding to a few 10 μm in this sample) identifies a spatial scale in the system where dynamics is coherent.[40]

applications, these fluctuations are caused by the variation of the scatterer positions because of translational Brownian motion or other motility processes accounting for the movement of the particle centers of masses. However, rotational motion of optically or shape anisotropic particles also produces fluctuations in the image intensity. These fluctuations contain quantitative information about the particles rotational motion and DDM has been recently proven to be able to extract such information and to probe simultaneously the translational and rotational diffusivities of optically anisotropic spherical particles.[42] The experimental setup is similar to the one used for the characterization of the viscoelastic constants in nematic liquid crystals[19] and coincides with a normal DDM setup (i.e., a microscope) equipped with two polarizing elements (i.e., a polarizing microscope). This variant of DDM has been thus named polarized DDM (p-DDM) and can be thought of as the extension to microscopy experiments of the well-known depolarized DLS (DDLS) technique, widely used for the assessment of the roto-translational diffusivity of anisotropic particles.[43] In general, the intermediate scattering function of a suspension of anisotropic particles exhibits a double-exponential relaxation: the two characteristic times of this relaxation are $\tau_1(q) = (D_T q^2 + 6D_R)^{-1}$ and $\tau_2(q) = (D_T q^2)^{-1}$, where D_T and D_R are the translational and rotational diffusivities of the particles, respectively. For large wave-vectors q (the regime typically probed by DDLS), these two modes are difficult to separate and polarizers are used to suppress the transmitted beam and to isolate the depolarized component of the scattered light, i.e., the one decaying with characteristic time $\tau_1(q)$. By contrast, in p-DDM experiments, the transmitted beam is used as a local oscillator and, in these conditions, both decay modes are probed and well separated (Fig. 7). p-DDM for the simultaneous determination of translational and rotational diffusion coefficients of optically anisotropic colloidal particles was demonstrated in Ref. 42, where particles with radius 185 nm were studied successfully at various volume fractions suggesting that

p-DDM can be a valid complement to DDLS and particle tracking in determining the roto-translational motility of particles. It is worth noting that the determination of the rotational diffusion coefficient with particle tracking cannot be performed in an automated fashion and, in general, constitutes quite a challenging feat. By contrast, p-DDM does not require any arbitrary input from users and is thus less subjected to bias. Compared with DDLS, p-DDM may more easily probe rotational motion of seed particles in laminar or turbulent flows and provide in turn space-resolved maps of the local fluid vorticity.
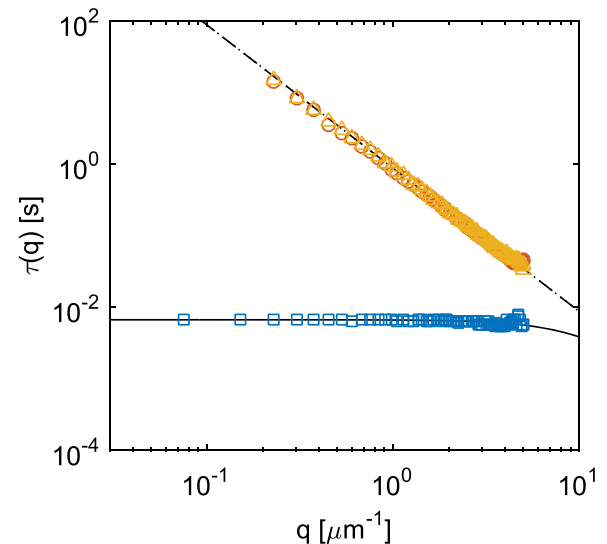

FIG. 7. Relaxation time as a function of the scattering wave-vector q obtained by using p-DDM (blue squares and orange circles) and bright-field DDM (yellow triangles) with a colloidal suspension (volume fraction 10^{-5}) of optically anisotropic spherical particles of radius 185 nm. Continuous and dashed lines are the best fitting curves to the theoretical expressions $\tau_1(q) = (D_T q^2 + 6D_R)^{-1}$ and $\tau_2(q) = (D_T q^2)^{-1}$, respectively, where D_T (D_R) is the translational (rotational) diffusivity of the particles. The best estimates for the diffusivities obtained with p-DDM are $D_T = 1.14 \pm 0.02$ μm^2 s^{-1} and $D_R = 25.1 \pm 1.0$ s^{-1}, whereas the bright-field DDM provides $D_T = 1.18 \pm 0.02$ μm^2 s^{-1} (dotted line).[42]

G. Microdynamics and arrest of coarsening during spinodal decomposition in thermoreversible colloidal gels

A relevant step forward in showing how DDM can be adapted to the "complex scenarios" envisioned near the end of Sec. II is represented by the work of Gao *et al.*[23] This work was the first to perform DDM measurements on colloidal gels, obtained by temperature quenching thermosensitive oil-in-water nanoemulsions prepared at volume fractions larger than the critical one. In this case, DDM was particularly useful to probe the multi-scale nature of dynamics during phase-separation, in particular the kinetic arrest of the bicontinuous structure formed by spinodal decomposition after the quench. Even though most of the DDM analysis performed was "standard," this work exemplifies many of the advantages of DDM compared to DLS and video particle tracking (VPT): the samples are turbid, prohibiting both DLS and confocal microscopy; no probe particles were present, preventing traditional VPT analysis; the experiments offer both a real-space and Fourier space representations that provide a clearer picture of the physics associated with heterogeneous dynamics. Complex dynami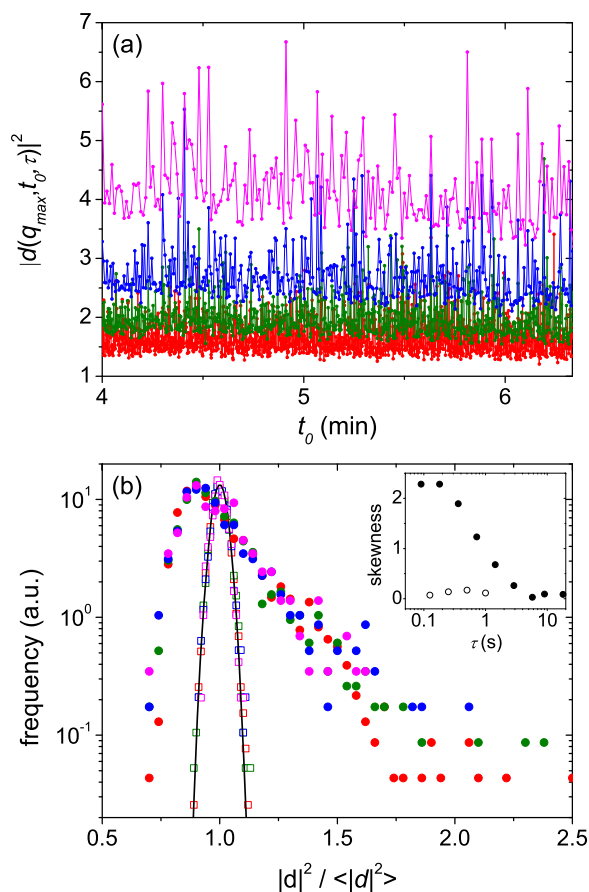cs was observed that was found to be described by a combination of a short-time exponential decay and long-time super-diffusive ballistic dynamics. A very interesting result presented by Gao *et al.* is a time-resolved[44] version of DDM, in which the instantaneous value $|d(\vec{q}, t_0, \tau)|^2$ of the intermediate scattering function before performing the ensemble average in Eq. (2), is used to probe the intermittent dynamics during gelation (Fig. 8).

To this aim, the fluctuations of $|d(\vec{q}, t_0, \tau)|^2$ at $q = q_{max}(t_0)$ are studied at several different lag times τ [Fig. 8(a)], where q_{max} is the wave-vector for which A(q) exhibits a maximum, which corresponds to the characteristic wavelength of the phase separating domains. Occasional excursions to high values are observed in Fig. 8(a), which are linked to intermittent rearrangements in the gel. Further insight into the intermittent dynamics was then obtained by examining the distributions of $|d|^2$ about its mean value $\langle |d|^2 \rangle$, which is reported in Fig. 8(b) together with results obtained with a dilute nanoparticle suspension [polystyrene beads, a = (95 ± 6) nm, 2.6 wt. % in water]. It can be appreciated that while the colloidal suspension exhibits a Gaussian distribution mirroring ergodicity, the distributions observed for the phase separating nanoemulsion deviate strongly from a Gaussian, as expected for intermittent dynamics that temporarily decrease correlations at short times.

IV. ESTABLISHED POINTS OF STRENGTHS AND LIMITING FACTORS

After almost ten years from its introduction, DDM has revealed many points of strength compared to other techniques, as well as some limiting factors. At a more general level, DDM represents a readily implemented technique that is extremely versatile and adaptable to almost any imaging system: bright-field,[11,16,21,45] wide-field and confocal[18,35] fluorescence,[26,37] dark-field,[17] phase-contrast,[24] DIC,[37] light-sheet,[25] reflection[37] and polarized[19,42] microscopy have been already used successfully on a variety of samples that include colloidal particles[11,16,21,26,27,32,46] and aggregates,[47] liquid crystals,[19] proteins,[45] bacteria,[18,24,48] algae,[24] vesicles,[37] actin,[37] and cilia.[40] It offers an immediate approach to the characterization of the type of motion from a study of the characteristic time $\tau(q)$ vs q, which in the most frequent cases can be used for particle sizing or for the determination of the swimming velocity for bacteria, algae, and micro-organisms.

In the context of microscopic dynamics probed by optical tools, compared to DLS, DDM offers a high-throughput, multi-q characterization of the dynamics of moving entities in a wave-vector range that extends typically down to 0.1 μm^{-1}. It can be set up (in bright-field) to sample a larger sample volume (plus, often, at higher concentrations because the depth of focus is exploited rather than the transmitted light path length) leading to much better statistics on sample dynamics for a given experimental sampling time. This value of the wave-vector, corresponds in aqueous samples to a scattering angle of $0.43°$ with a He–Ne laser source (wavelength 633 nm). This angle is one order of magnitude below the smallest scattering angle accessible with commercial scattering instruments (typically of the order of $10°$-$15°$), which hardly can access smaller angles due to the presence of stray light scattered for instance

FIG. 8. Intermittent dynamics of a gelling nanoemulsion probed by time-resolved DDM. (a) $|d(\vec{q}, t_0, \tau)|^2$ is plotted at τ = 0.09 (red), 0.18 (green), 0.36 (blue), and 0.72 s (magenta) as a function of aging time t_0. (b) Normalized distribution of $|d|^2$ for gelling nanoemulsions (closed symbols) and a dilute nanoparticle suspension (open symbols), the latter exhibiting Gaussian behaviour (solid line), whereas the former being non-Gaussian. The inset represents the skewness of the distributions in (b). Adapted with permission from Gao *et al.*, Soft Matter **11**, 6360 (2015). Copyright 2015 The Royal Society of Chemistry.

from imperfections (e.g., dust, scratches, and dirt) along the optical trains or in the sample cell. DDM is rather insensitive to this stray light that represents a static contribution in the microscope images and is thus subtracted off with the differential analysis. In fact, this partial insensitivity means that both the optical quality of the surfaces of which the sample cell is made and to some extent their cleaning do not need to be at the same level as in DLS experiments. It remains however true that the sample cell should preferably contain only the sample of interest since moving contaminants will likely produce a non-negligible signal in DDM experiments, like DLS. In spatially inhomogeneous samples, DDM can probe different fields of view (the equivalent of scattering volumes in DLS experiments), which gives another important advantage over DLS, where selecting different scattering volumes is challenging and time consuming, when it is even possible. As far as limitations are concerned, DDM camera detectors do not yet compare with the performances of photomultiplier tubes and avalanche photodiodes used in DLS, neither in terms of speed nor of sensitivity to small signals. In this respect, it must be stressed that at least in its homodyne configuration, DLS measures the intensity of the scattered light on an ideally dark background, whereas DDM analyzes the small fluctuations caused by the scattered light on top of the bright transmitted beam, a configuration which is more similar to the heterodyne DLS configuration. A positive consequence of this detection scheme is that in DDM, as well as in heterodyne DLS, the fluctuating signal of which the temporal correlation properties are calculated is proportional to the scattering field rather than to the scattering intensity. In principle, this offers an advantage for particle sizing applications where the size-dependence of the scattering intensity is challenging (as the particle radius to the sixth power in the Rayleigh regime) and is mitigated by working with the electric field.

Compared to video particle tracking (VPT), there are three main advantages of DDM when it comes to image analysis. The first two relate to sample conditions and open up new types of experiment: (i) that there is *no need for segmentation* of the images, which makes it possible to study samples where the particles are very small and (ii) *no need for tracking features* across frames, which means much denser systems can be measured. The other key advantage (iii) is that *DDM requires no user-defined parameters* once a family of fitting functions is assigned (a modest restriction on the dynamics that is searched for) and may be thus entirely automatic and unbiased. In particular, related to (iii), we stress the fact that VPT requires user choices at almost every step of the image analysis: for an object to be tagged as a particle or feature of interest, the user must choose, for example, its minimum and maximum lateral size, its minimum brightness, the maximum displacement allowed between two successive frames, and the particle trajectory length value below which a trajectory is discarded from the final analysis (these are only some of the choices that the user needs to operate). This might partially explain why VPT is mostly used in academic research laboratories and has not been adopted in industrial environments where automation and standardization are strong requirements. In this respect, DDM might represent an interesting option with the caveat that for "unsupervised" analysis, one needs to be sure that the sample

dynamics are purely from the phenomenon of interest (e.g., no "dirt") because there is not a chance later to clean up the results. Also, VPT used properly is a very powerful technique that enables a complete sorting (e.g., in size or velocity) of the moving entities within a sample (e.g., a cell), whereas DDM is in this respect more similar to DLS in its need to invert the intermediate scattering function to obtain a probability function distribution (e.g., of size or velocity). For moderately polydisperse samples, a cumulant analysis such as the one used in DLS has been proven to be applicable,[42,45] and there are no barriers to employing more complex inversion procedures, as we will discuss further below. It is also worth mentioning that VPT may pose also some constraints on the imaging methods and/or on the samples. For instance, a typical ideal configuration for VPT experiments makes use of epifluorescence (or confocal) microscopy in order to increase the signal-to-noise ratio and make the suspending fluid invisible to better track the colloidal particles. By contrast, since DDM effectively probes signals that are way smaller than the noise, the user has more freedom in the choice of the experimental parameters.

PIV is, in our opinion, the technique that shares with DDM the largest number of similarities. It is typically performed with images acquired at a fixed frame rate with the same type of pixelated detectors. It also calculates some sort of cross correlation between successive images to evaluate the displacement and the velocity either on the whole image or, more frequently, on some regions of interest in which the original image is divided. For both DDM and PIV, there is a trade-off of spatial resolution vs. the range of scales that one measures. The typical output of the PIV analysis is thus a velocity (or displacement) map with the resolution of a few pixels. PIV is a well-established method that has been fine-tuned during the years and nowadays can even operate in real-time. By contrast, DDM is still in its young age and real-time analysis has not yet been achieved, even though GPU accelerated versions of the differential dynamic algorithm have been successfully implemented,[18,49] as well as efficient schemes for data sampling that can probe fast dynamics at a low average data acquisition rate.[50] A big limitation of PIV compared to DDM is that being inherently conceived for assessing velocity, it is not the right tool for mapping disordered forms of motility such as Brownian motion, even though in principle this is possible.

V. PERSPECTIVE AND FUTURE CHALLENGES

We can expect in just a few years to be able to run DDM in real time on video feeds of over 100 fps (this could be on a CPU or GPU, requiring ideally 32 GB of RAM); this would be the ultimate application of DDM avoiding even the need for the storage of large quantities of data, reducing the image flow to its intrinsic dynamical information content, providing real-time physical measurement, and allowing experimental design based on advanced imaging-driven triggers.

Given the very challenging diversity in biological systems like real tissue surfaces or cell monolayers, observed in optical microscopy, the automation, robustness, and standardization of DDM are extremely appealing. DDM represents a very powerful and informative video analysis approach, which in our hands has become the first routine analysis carried out

systematically on most experiments involving dynamics of living matter. Clearly, DDM cannot be thought of as the only image analysis tool: information that is typically related to heterogeneity or correlated to other detailed spatial features then does require cell segmentation or some other form of image feature analysis. In the context of monitoring motility of microorganisms, the groundwork for using DDM is in the literature, and we can imagine that the technique can be deployed in health-related applications (sperm motility testing for fertility and bacteria motility for screening in various infections), in on-line monitoring of bioreactors or waste management systems.

In non-biological soft materials, such as complex fluids, DDM has again clear areas of application that exploit automation and standardization. Particle sizing, in the range from few tens of nanometers to a micrometer, can very effectively be carried out with DDM, with the many advantages described in this review over DLS. In the presence of polydispersity ultimately, the same challenges well known in DLS will show up, and users will have to face inversion of data, for example, through CONTIN algorithm:[51] we have described many DDM advantages, from the decreased intensity-size dependence, to the cost of apparatus and typically stronger statistics from larger sample volumes probed. The application of DDM as a microrheology tool, using tracer particles but avoiding the limitations associated to tracking them, is one of the avenues being pursued by ourselves and others. The information extracted of DDM cuts across from what can be achieved in particle tracking or DLS, with much simpler apparatus and analysis pipelines.

Finally and particularly with multiscale DDM analysis, a very complete picture of dynamics decomposed by length scale can be obtained: this will be very powerful in the context of glassy materials and heterogeneous dynamics,[52] for which distinguishing features such as collective rearrangements, giant fluctuations, intermittency, dynamical heterogeneity are observed, also for biological systems. In this context, and in particular for biological systems that are typically studied with microscopes,[53–55] it is desirable to obtain simple and quantitative indicators of the proximity to this transition. It is now accepted that high-order spatio-temporal dynamic correlation functions are needed, such as the four-point dynamic correlation function $G_4(r; t)$ or the dynamic susceptibility $\chi_4(t)$, which is the space integral of G_4.[56] In this respect, comparing real-space and Fourier-space techniques teaches an interesting lesson: while visualizing intermittent, collective motility events is easier in real-space, the calculation of the dynamic susceptibility is more immediate in the reciprocal space, where however no visual information is available. DDM may offer the needed intermediate perspective, and an important step in this direction has been recently made by Pastore *et al.* with the introduction of Difference Variance Analysis (DVA).[57] As in DDM, the key idea is that taking differences between images separated by a variable delay τ is a direct way of isolating only the contribution of moving entities in the sample. A first quantification of the sample dynamics can be thus obtained by simply calculating the variance of these difference images as a function of τ,[11] which is equivalent to averaging the DDM dynamics of all the probed wave-vectors with a weight function

that is given by the amplitude $A(q)$ in Eq. (3). In the presence of dynamic heterogeneity and for a fixed τ, this variance exhibits an intrinsic, ensemble variability that depends on τ and exhibits a maximum for τ of the order of the characteristic time τ_c of the cooperative relaxation of density. Pastore *et al.* showed that the difference images are the ideal tool to single out this variability and, more generally, the existence of dynamical heterogeneity. In addition, they suggest a recipe for calculating in a straightforward way the dynamic susceptibility $\chi_4(\Delta t)$ from these difference images. It is worth noting that the applicability of this simple approach might be limited to systems for which the amplitude $A(q)$ exhibits a maximum around a wave-vector q corresponding to a length scale in real space of the order of the typical inter-particle distance. Nevertheless, it is likely that a full extension to a wave-resolved analysis will be more generally applicable to arbitrary systems.

We have focused this perspective review on DDM in the context of microscopic dynamics, considering biological and soft materials where the typical length scales are of the order of micrometers and typical time scales from milliseconds to hours. This is where the technique has been applied so far. However, nothing in the DDM approach ties it down to the realm of microscopy; rather, DDM works in the more general world of video imaging. Future applications of DDM will surely extend well beyond the biological/colloidal systems. The robustness and automation will be very appealing to the analysis of digital video feeds in crowd monitoring, analysis of ocean waves, ice flows, or terrestrial strain patterns from satellite feeds where the length scales and time scales could be completely different from the physical systems described here.

ACKNOWLEDGMENTS

[1]B. Berne and R. Pecora, *Dynamic Light Scattering: With Applications to Chemistry, Biology, and Physics* (Dover Publications, 2000).

[2]B. Chu, in *Soft-Matter Characterization*, edited by R. Borsali and R. Pecora (Springer Netherlands, Dordrecht, 2008), pp. 335–372.

[3]W. Brown, *Dynamic Light Scattering: The Method and Some Applications* (Clarendon Press, 1993).

[4]T. Kanade, Z. Yin, R. Bise, S. Huh, S. Eom, M. F. Sandbothe, and M. Chen, in *2011 IEEE Workshop on Applications of Computer Vision* (IEEE, 2011), p. 374.

[5]E. Meijering, IEEE Signal Process. Mag. **29**, 140 (2012).

[6]S. Dimopoulos, C. Mayer, F. Rudolf, and J. Stelling, Bioinformatics **30**, 2644 (2014).

[7]T. A. Waigh, Rep. Prog. Phys. **79**, 074601 (2016).

[8]J. Westerweel, G. E. Elsinga, and R. J. Adrian, Annu. Rev. Fluid Mech. **45**, 409 (2013).

[9]J. P. Butler, I. M. Tolić-Nørrelykke, B. Fabry, and J. J. Fredberg, Am. J. Physiol.: Cell Physiol. **282**, C595 (2002).

[10]B. Sabass, M. L. Gardel, C. M. Waterman, and U. S. Schwarz, Biophys. J. **94**, 207 (2008).

[11]R. Cerbino and V. Trappe, Phys. Rev. Lett. **100**, 188102 (2008).

[12]R. Cerbino and A. Vailati, Curr. Opin. Colloid Interface Sci. **14**, 416 (2009).

[13]F. Giavazzi and R. Cerbino, J. Opt. **16**, 083001 (2014).

[14]F. Croccolo, D. Brogioli, A. Vailati, M. Giglio, and D. S. Cannell, Appl. Opt. **45**, 2166 (2006).

[15]F. Croccolo, D. Brogioli, A. Vailati, M. Giglio, and D. S. Cannell, Phys. Rev. E **76**, 041112 (2007).

[16]F. Giavazzi, D. Brogioli, V. Trappe, T. Bellini, and R. Cerbino, Phys. Rev. E **80**, 031403 (2009).

[17]A. V. Bayles, T. M. Squires, and M. E. Helgeson, Soft Matter **12**, 2440 (2016).

[18]P. J. Lu, F. Giavazzi, T. E. Angelini, E. Zaccarelli, F. Jargstorff, A. B. Schofield, J. N. Wilking, M. B. Romanowsky, D. A. Weitz, and R. Cerbino, Phys. Rev. Lett. **108**, 218103 (2012).

[19]F. Giavazzi, S. Crotti, A. Speciale, F. Serra, G. Zanchetta, V. Trappe, M. Buscaglia, T. Bellini, and R. Cerbino, Soft Matter **10**, 3938 (2014).

[20]F. Giavazzi, G. Savorana, A. Vailati, and R. Cerbino, Soft Matter **12**, 6588 (2016).

[21]D. Germain, M. Leocmach, and T. Gibaud, Am. J. Phys. **84**, 202 (2016).

[22]P. Cicuta and A. M. Donald, Soft Matter **3**, 1449 (2007).

[23]Y. Gao, J. Kim, and M. E. Helgeson, Soft Matter **11**, 6360 (2015).

[24]V. A. Martinez, R. Besseling, O. A. Croze, J. Tailleur, M. Reufer, J. Schwarz-Linek, L. G. Wilson, M. A. Bees, and W. C. K. Poon, Biophys. J. **103**, 1637 (2012).

[25]D. M. Wulstein, K. E. Regan, R. M. Robertson-Anderson, and R. Mcgorty, Opt. Express **24**, 20881 (2016).

[26]K. He, M. Spannuth, J. C. Conrad, and R. Krishnamoorti, Soft Matter **8**, 11933 (2012).

[27]K. He, F. Babaye Khorasani, S. T. Retterer, D. K. Thomas, J. C. Conrad, and R. Krishnamoorti, ACS Nano **7**, 5122 (2013).

[28]A. Dehaoui, B. Issenmann, and F. Caupin, Proc. Natl. Acad. Sci. U. S. A. **112**, 12020 (2015).

[29]J. Hallett, Proc. Phys. Soc. **82**, 1046 (1963).

[30]A. F. Collings and N. Bajenov, Metrologia **19**, 61 (1983).

[31]J. Kestin, N. Imaishi, S. H. Nott, J. C. Nieuwoudt, and J. V. Sengers, Phys. A **134**, 38 (1985).

[32]J. D. C. Jacob, K. He, S. T. Retterer, R. Krishnamoorti, and J. C. Conrad, Soft Matter **11**, 7515 (2015).

[33]J. C. Crocker and D. G. Grier, J. Colloid Interface Sci. **179**, 298 (1996).

[34]N. L. Thompson, *Topics in Fluorescence Spectroscopy* (Kluwer Academic Publishers, Boston, 2002), pp. 337–378.

[35]T. Sentjabrskaja, E. Zaccarelli, C. De Michele, F. Sciortino, P. Tartaglia, T. Voigtmann, S. U. Egelhaaf, and M. Laurati, Nat. Commun. **7**, 11133 (2016).

[36]D. Wirtz, Annu. Rev. Biophys. **38**, 301 (2009).

[37]M. Drechsler, F. Giavazzi, R. Cerbino, and I. M. Palacios, e-print bioRxiv 098590 (2017).

[38]M. E. Quinlan, Annu. Rev. Cell Dev. Biol. **32**, 173 (2016).

[39]M. Almonacid, W. W. Ahmed, M. Bussonnier, P. Mailly, T. Betz, R. Voituriez, N. S. Gov, and M.-H. Verlhac, Nat. Cell Biol. **17**, 470 (2015).

[40]L. Feriani, M. Juenet, C. J. Fowler, and N. Bruot, Biophys. J. **113**, 109 (2017).

[41]N. Bruot and P. Cicuta, Annu. Rev. Condens. Matter Phys. **7**, 323 (2015).

[42]F. Giavazzi, C. Haro-Pérez, and R. Cerbino, J. Phys.: Condens. Matter **28**, 195201 (2016).

[43]V. Degiorgio, R. Piazza, T. Bellini, and F. Mantegazza, *Light Scattering and Photon Correlation Spectroscopy* (Springer Netherlands, Dordrecht, 1997), pp. 7–21.

[44]A. Duri, H. Bissig, V. Trappe, and L. Cipelletti, Phys. Rev. E **72**, 051401 (2005).

[45]M. S. Safari, M. A. Vorontsova, R. Poling-Skutvik, P. G. Vekilov, and J. C. Conrad, Phys. Rev. E **92**, 042712 (2015).

[46]M. Reufer, V. A. Martinez, P. Schurtenberger, and W. C. K. Poon, Langmuir **28**, 4618 (2012).

[47]F. Ferri, A. D'Angelo, M. Lee, A. Lotti, M. C. Pigazzini, K. Singh, and R. Cerbino, Eur. Phys. J.: Spec. Top. **199**, 139 (2011).

[48]L. G. Wilson, V. A. Martinez, J. Schwarz-Linek, J. Tailleur, G. Bryant, P. N. Pusey, and W. C. K. Poon, Phys. Rev. Lett. **106**, 018101 (2011).

[49]G. Cerchiari, F. Croccolo, F. Cardinaux, and F. Scheffold, Rev. Sci. Instrum. **83**, 106101 (2012).

[50]A. Philippe, S. Aime, V. Roger, R. Jelinek, G. Prévot, L. Berthier, and L. Cipelletti, J. Phys.: Condens. Matter **28**, 075201 (2016).

[51]S. W. Provencher, Comput. Phys. Commun. **27**, 229 (1982).

[52]L. Berthier, G. Biroli, J. P. Bouchaud, L. Cipelletti, and W. van Saarloos, *Dynamical Heterogeneities in Glasses, Colloids, and Granular Media* (Oxford University Press, 2011).

[53]T. E. Angelini, E. Hannezo, X. Trepat, M. Marquez, J. J. Fredberg, and D. A. Weitz, Proc. Natl. Acad. Sci. U. S. A. **108**, 4714 (2011).

[54]J.-A. Park, J. H. Kim, D. Bi, J. A. Mitchel, N. T. Qazvini, K. Tantisira, C. Y. Park, M. McGill, S.-H. Kim, B. Gweon, J. Notbohm, R. Steward, Jr., S. Burger, S. H. Randell, A. T. Kho, D. T. Tambe, C. Hardin, S. A. Shore, E. Israel, D. A. Weitz, D. J. Tschumperlin, E. P. Henske, S. T. Weiss, M. L. Manning, J. P. Butler, J. M. Drazen, and J. J. Fredberg, Nat. Mater. **14**, 1040 (2015).

[55]C. Malinverno, S. Corallino, F. Giavazzi, M. Bergert, Q. Li, M. Leoni, A. Disanza, E. Frittoli, A. Oldani, E. Martini, T. Lendenmann, G. Deflorian, G. V. Beznoussenko, D. Poulikakos, K. H. Ong, M. Uroz, X. Trepat, D. Parazzoli, P. Maiuri, W. Yu, A. Ferrari, R. Cerbino, and G. Scita, Nat. Mater. **16**, 587 (2017).

[56]L. Berthier, Physics **4**, 42 (2011).

[57]R. Pastore, G. Pesce, and M. Caggioni, Sci. Rep. **7**, 43496 (2017).